and Pathos DELTA (Milestone Medical Technologies). Quality assessments were made of ease of embedding and microtome sectioning and histopathologic variables of hematoxylin and eosin staining intensity, homogeneity, nuclear preservation, nucleolar prominence, autolysis or thermal artifact. Microscopic sections were evaluated by one GU pathologist. Microscopic quality was scored on a 10-part scale.

Results: With the exception of the FixMate heated and timed fixation tests at 37°C and 45°C, all combinations gave inconsistent and spotty unacceptable, suboptimal to good microscopic preparations no matter the variable manipulated. The higher 50°C test of heated formalin fixation resulted in an artifact of nuclear chromatin that was dark and smudgy. The histologic quality at 37°C was judged slightly superior to 45°C. No significant difference in quality of tissue microtomy or histologic preparation was noted for either microwave tissue processor.

Conclusions: Enhanced consistency in the quality of histologic preparations using rapid microwave processors is obtained when prostate needle biopsy fixation is standardized with controlled time and temperature of fixation.

1947 Integration of Microwave Technology To Reduce Fixation and Processing Time of Robotic Prostatectomy Specimens for Whole Mount Examination.

RJ Zarbo, R Varney, O Alassi, N Main, S Richard, R D'Angelo, B Mahar, D Lubensky, ON Kryvenko, A Ormsby, S McMahon, N Draga, N Gupta. Henry Ford Health System, Detroit, MI.

Background: Using the Lean tool of value stream mapping, we identified the preanalytic phase of processes from specimen receipt to tissue processing as the major source of time delay and non-value added effort in the value stream of whole mount prostatectomy evaluation.

Design: We targeted intact gland formalin fixation and tissue processing of whole mount (WM) sections. The initial condition consisted of 50-100ml formalin needle injection of intact robotic prostatectomies using a fine needle. Intact glands were then fixed overnight in 32 oz. formalin for avg. 15.8 hours. Glands were entirely sectioned at 4mm thickness and WM sections were fixed for 9 hrs. in macro-cassettes (LPC1000, Cancer Diagnostics Inc) and processed for 16.5 hrs. in a VIP 300E processor (Sakura Finetek USA, Inc, Torrance, CA). The redesigned condition retained formalin injection of glands that were then fixed intact in 32 oz. of formalin for 30 min. followed by microwave fixation in 32 oz. of formalin in a microwave processor (Model EBS42850, EBSciences, East Granby, CT) at 450W for 6 min. at 50C°. Glands over 50 grams were held for 15 additional min. in formalin at room temperature then microwaved again for 3.5 min. WM sections were then fixed in macro-cassettes for an additional 2 hrs. at room temperature. Total fixation time in the redesigned process was 2.53 hrs. WM sections were processed in 7 hrs. in macro-cassettes in a Pathos DELTA microwave processor (Milestone Medical Technologies, Inc, Kalamazoo, MI/Sirasole, Italy). Baselines were from 20 robotic prostatectomies. New conditions were tested on 5 autopsy and 10 clinical glands.The latter were parallel tested with WM slices from each gland in the VIP and Pathos DELTA processors. All microscopic sections were assessed by one GU pathologist.

Results: With process redesign fixation time was reduced by 90% from 24.8 to 2.53 hrs. Integrating microwave technology in tissue processing reduced processor time by 58% from 16.5 to 7 hrs. Overall, 32 hrs. of non-value added time waste was removed from the front end processes resulting in a 77% reduction from 41.3 to 9.5 hrs. Pathologic examination showed no significant variations in quality related to H&E staining, homogeneity, crust/edge effect, completeness of margins, nuclear preservation, autolysis or thermal artifact.

Conclusions: Lean process redesign targeting intact prostate gland fixation and integration of microwave technology in radical prostatectomy processing can be of great benefit in addressing total timeliness of pathologic reporting.

1948 Nottingham-Defined Mitotic Score: Comparison to Visual and Image Cytometric Phosphohistone H3 Labeling Indices and Correlation with Oncotype DX Recurrence Score.

B Zbytek, C Cohen, AJ Page, AL Adams. Emory University, Atlanta, GA.

Background: Prognosis of breast cancer patients has been determined traditionally by lymph node status, tumor size, and histologic grade. In recent years the Oncotype DX Recurrence Score (RS) assay has emerged as a costly adjunct prognostic tool. Markers of proliferation play a large role in determination of RS, and we have shown previously that immunohistochemical expression of proliferation markers Ki-67 and phosphohistone H3 (PPH3) correlates with RS. Our current goal is comparison of the hematoxylin-and-eosin (H&E) mitotic score, defined by the Nottingham grading system, to anti-PPH3 mitotic figure labeling assessed by both visual and automated image analysis and correlation of mitotic score results with RS.

Design: Estrogen receptor-positive breast carcinomas from 138 patients with Oncotype DX testing were selected. A representative H&E-stained tumor section was evaluated. Mitoses were counted per 10 HPF and tumors graded using the Nottingham criteria by one pathologist in accordance with CAP-recommended mitotic count cutoffs for a field diameter of 0.55 mm. An additional section was immunostained with PPH3 antibody (Dako). PPH3 mitotic scores were determined visually per 10 HPF and by the Automated Cellular Imaging System III (Dako) in 10 "hotspots". Statistical analysis was performed using univariate tests and Pearson's correlation coefficient.

Results: There was a significant association between H&E mitosis score and RS ($p<0.001$, $R=0.34$).

Mitotic score	Oncotype DX Recurrence Score		
	Low	Intermediate	High
1	65 (56%)	43 (37%)	9 (7%)
2	6 (32%)	4 (21%)	9 (47%)
3	0 (0)	1 (50%)	1 (50%)

RS associations with visual and automated PPH3 mitotic scores were also significant (visual: $p<0.001$, $R=0.32$; automated: $p<0.005$, $R=0.25$). The three methods of mitotic score assessment were strongly associated with each other.

Method	Pearson's R	p
Mitotic Score: H&E vs. PPH3 Visual	.41	<0.001
Mitotic Score: PPH3 Visual vs. Automated PPH3	.71	<0.001
Tumor Grade Using H&E Mitotic Score vs. PPH3 Visual	.81	<0.001

Conclusions: The Nottingham-derived H&E mitotic score is significantly associated with RS. There is significant correlation between mitotic scores determined by H&E and by PPH3 labeling assessed visually and by imaging. There is significant correlation between grades determined by H&E and PPH3 labeling. Mitotic score by any of the three methods studied may be useful in assessing tumor grade, proliferation,and prognosis.

Ultrastructural

1949 Unique Ultrastructural Features in Diagnosis of Hepatocellular Carcinoma in Fine Needle Aspiration Cytology Specimen.

A Abdul-Nabi, G Sidhu, N Cassai, J Liao, G-Y Yang. Northwestern University, Chicago, IL; NYU School of Medicine, NewYork, NY.

Background: Fine needle aspiration cytology (FNAC) has been widely used as a minimally invasive and rapid method of diagnosis of primary or metastatic hepatic masses. But its sensitivity appears low (67% to 93%) and a negative result does not exclude malignancy. Although immunohistochemistry is commonly used as an ancillary test, definitive biomarker for hepatocellular carcinoma (HCC) is lacking. Many studies have shown that electron microscopy (EM) has the precise ability in identifying normal and neoplastic hepatocyte ultrastructurally, but its use is still limited. Our study aims to characterize unique ultrastructural features of HCC and evaluate its usefulness as a diagnostic tool in FNAC.

Design: FNAC specimens from 67 cases of HCC with different degrees of differentiation confirmed histopathologically by core-needle biopsy or hepatoectomy were collected between 1993-2003. Parallel FNAC specimens were submitted for EM examination.

Results: Among 67 HCC cases, 95% (64/67) of the cases was confirmed the FNAC diagnosis of HCC. In 3 discrepancy cases, EM established a definitive diagnosis of metastatic colonic adenocarcinoma, and the two other cases EM diagnostic accuracy was limited by failure to obtain adequate sample. The following unique ultrastructural features in diagnosing 64 HCC cases were identified as: 1) Capillarization which were trabecular neoplastic hepatocytes surrounded by fenestrated or not separated endothelia with continuous basal lamina (Fig.1A); 2)altered bile canaliculi which commonly formed by more than three neoplastic hepatocytes and usually contained bile material (Fig.1B); 3) high atypical round to irregular shape nuclei with very large, ropy nucleoli that had nucleolonema (Fig.1C). Intranuclear cytoplasmic inclusions and giant mitochondria were also observed in the neoplastic cells.

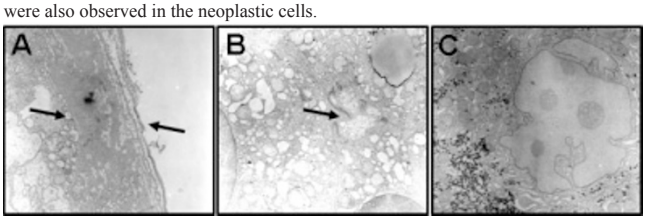

Conclusions: Our results indicate that HCC displays unique ultrastructural features, which can be used as a reliable and accurate diagnostic tool for HCC in limited FNAC. EM is superior to FNAC in determining the tumor origin and in making more definitive diagnosis.

1950 "Cilia Metaplasia" in Renal Transplant Biopsies with Acute Tubular Injury.

HS Desai, JP Roszka, ML Kaiser, KL Dundas, MT Rooney, PL Zhang. William Beaumont Hospital, Royal Oak, MI.

Background: Primary cilia are hair-like organelles singly distributed along the apical surface of proximal and distal nephron tubules. They are known to play a mechanosensation role in tubular differentiation. A recent study demonstrated increased length of cilia in renal transplantation with acute tubular injury (ATI), using immunofluorescent method against alpha-tubulin, as an indicator of injury and repair (J Am Soc Nephrol 2009: 20: 2147-2153). In our study we used electron microscopy (EM) to evaluate cilia changes in acute tubular injury (ATI) in both transplant and native biopsies.

Design: Three groups of cases were included: control group 1- native biopsies without major changes in renal tubules; study group 2- native biopsies with prominent ATI, and study group 3- renal transplant biopsies with prominent ATI (delayed renal function group). Extensive search for ciliary structures along renal tubules (at least 10 15 fields at 6,500 magnification) was conducted in each case. When cilia were identified, high magnification (up to 130,000) was used to obtain images for detailed ultrastructural study. The search for cilia was focused on proximal tubular areas with injured (diminished) apical microvilli.

Results: Singly located cilia were found in 3/19 specimens in control group 1, 4/18 in group 2 (native ATI), and 6/24 in group 3 (transplant ATI). Importantly, there were clusters of cilia in proximal tubules with markedly diminished apical microvilli in 3/25 biopsies from two patients in group 3, but none from groups 1 and 2. The clusters of cilia ranged from 6 to 15 individual cilia along the apical surface with diminished apical microvilli.

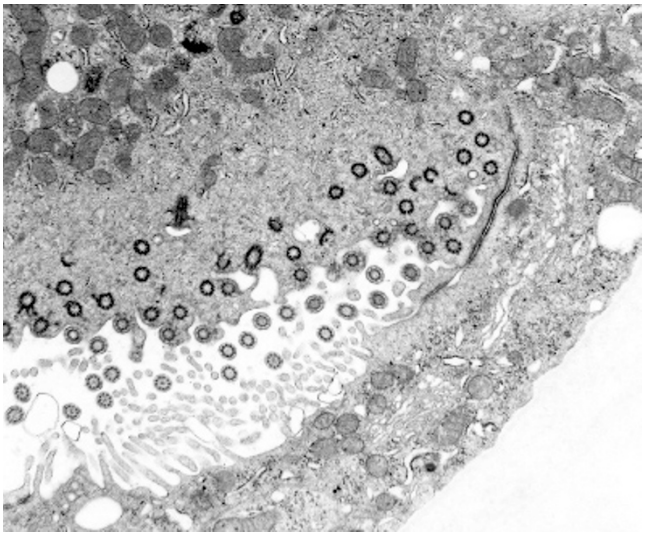

Under high magnifications, the cilia demonstrated 9 pairs of peripheral microtubules without central two singlet microtubules, consistent with primary cilia (9 + 0) rather than motile cilia (9 + 2).

Conclusions: Using EM, we found clusters of cilia in proximal tubules with remarkable apical microvillar injury in 3 biopsies from renal transplants with ATI; we name this finding as "cilia metaplasia." The "metaplastic" cilia are primary cilia (9 + 0) and may be an index for the repairing process.

1951 Ultrastructural Evidence of Autophagy in Cerebral Capillary Pericytes in Notch3 Mutant Transgenic Mice.

X Gu, X Liu, L-R Zhao. Louisiana State Universtiy at Shreveport.

Background: Notch3 encodes a transmembrane receptor. Postnatal expression of Notch3 is predominantly in vascular smooth muscle cells (VSMCs) and pericytes. In cerebral autosomal dominant arteriopathy with subcortical infarcts and leukoencephalopathy and in animal models, Notch3 mutation resulted in VSMC degeneration and the accumulation of granular osmiophilic material (GOM) in vascular walls. Notch3 mutation associated cerebral capillary pathology has not been described. We have studied the ultrastructural morphology of cerebral capillaries in aged Notch3 mutant transgenic mice and have identified evidence of autophagy (type 2 apoptosis) in capillary pericytes.

Design: Sections of brain from four controls and ten Notch3 mutant transgenic mice (22-month old) were fixed and sectioned for electron microscopy (EM) according to standard techniques. An average 20-40 capillaries in the cerebral cortex in each section were examined.

Results: In controls, no capillaries showed pericyte autophagy. In Notch3 mutant mice, 5-10% of the capillaries revealed pericyte autophagy. Different stages of autophagic vacuoles presented in these pericytes (figures 1, 2). No GOM was identified in the pericytes/vascular walls.

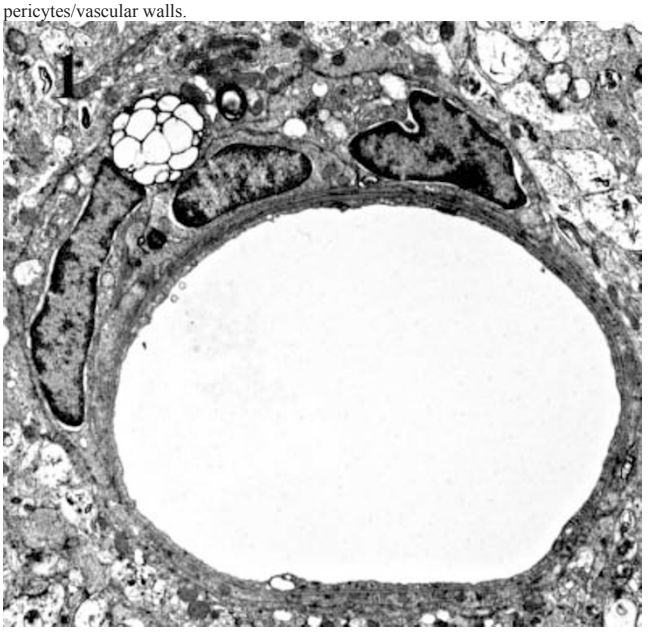

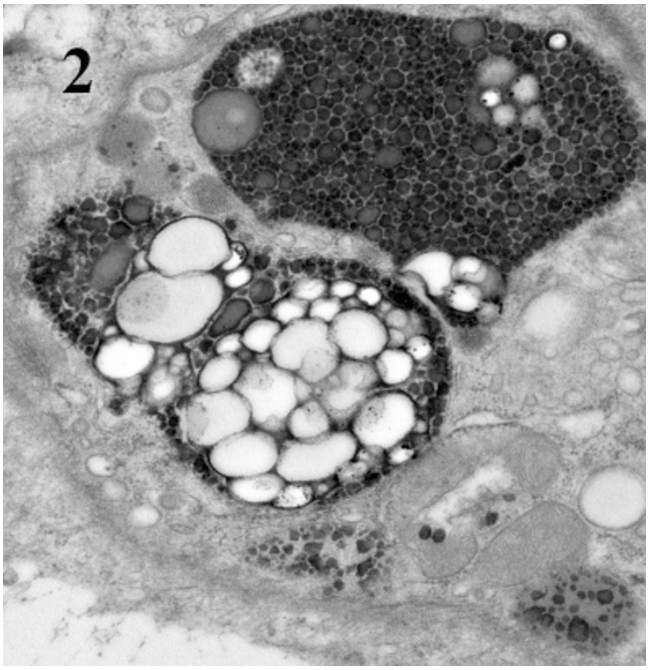

Conclusions: EM revealed autophagy in cerebral capillary pericytes in Notch3 mutant transgenic mice. To best of our knowledge, this is the first report to describe autophagy in the pericytes associated with Notch3 mutation. In contrast to previous studies of arterioles, there was no GOM accumulation in the pericytes and capillary walls. These findings suggest that abnormal Notch3 signaling results in type 2 apoptosis in cerebral capillary pericytes. Capillary pericyte autophagy may lead to capillary injury, microcirculatory dysfunction, hypoperfusion and white matter degeneration.

1952 Pulmonary Interstitial Glycogenosis: Review of Histopathologic, Immunocytochemical and Ultrastructural Features.

J Hicks, C Langston, E Wartchow, G Mierau. Texas Children's Hospital & Baylor College of Medicine, Houston; The Children's Hospital, Denver, CO.

Background: Pulmonary interstitial glycogenosis (PIG) is a recently described idiopathic childhood interstitial lung disease, based upon identifying glycogen-laden mesenchymal cells in the alveolar interstitium. PIG may be an isolated finding, or associated with disorders of deficient lung growth or development (up to 40% of cases). Infants with PIG tend to have a more favorable prognosis with or without corticosteroid therapy compared with children with chronic pneumonitis of infancy.

Design: Pathology archive review of 2 pediatric hospitals identified 18 infants that were diagnosed with PIG. The study population was comprised of 10 females and 8 males with an age range of 2 weeks to 4 months. The typical clinical scenario was tachypnea, hypoxemia, and diffuse interstitial infiltrates with overinflated lungs on radiologic examination. The lung biopsies from these patients had routine histologic examination, PAS and PAS-diastase staining, vimentin and CD68 immunostaining, and electron microscopic examination performed.

Results: The lung biopsies typically showed alveolar interstitial widening with increased cellularity. The increased cellularity was not due to inflammatory cells, but associated with intersitial mesenchymal cells. These cells were immunoreactive with vimentin, and lacked CD68 reactivity and were not histiocytes. Typically, PAS positive, diastase-sensitive material indicative of glycogen was noted within the cytoplasm of interstitial mesenchymal cells. However, the detection by PAS was inconsistent, most likely due to loss of glycogen with formalin fixation. Electron microscopy demonstrated readily that the spindle-shaped intersitial cells were engorged with monoparticulate glycogen and accounted for the interstitial widening. Other findings included concomitant lung injury or remodeling associated with alveolar growth abnormalities.

Conclusions: PIG is associated with glycogen accumulation in the interstitial mesenchymal cells and has been postulated to represent an abnormality of lung cytodifferentiation or interstitial cell maturation. There is no association with systemic glycogen storage disease. Ultrastructural examination can facilitate recognition of PIG. PIG should be considered with an neonate or infant that has a bronchopulmonary-like clinical presentation when intubation is not necessary and when infectious and inflammatory etiologies have been excluded. It is important to recognize PIG because it tend to have a more favorable outcome than chronic pneumonitis of infancy.

1953 Inhibition of Osteopontin Affects Glomerular Sclerosis and Crescent Formation in Animal Model of Anti-Glomerular Basement Membrane Disease.

J Hicks, J Wu, J Barrish, S-H Zhu, R Nichols, Y-H Lou. Texas Children's Hospital and Baylor College of Medicine, Houston; University of Texas Health Science Center at Houston.

Background: Osteopontin (OPN) is an integrin-binding extracellular membrane glycophosphoprotein with a role in inflammation, autoimmunity and fibrosis. Glomerular OPN is upregulated in progressive renal failure. Anti-OPN antibody treatment is associated with decreased proteinuria, improved renal function and decreased interstitial fibrosis.

Design: An established rat mode for autoimmune anti-glomerular basement membrane disease (Anti-GBM) induced by immunization with a T-cell epitope pCol(28-40) peptide derived from alpha3 Type IV collagen chain or by transfer of Col4alpha3-specific T-cells was employed to induce glomerular disease. With this model, there are two distinct stages of disease induction: 1) CD4 T-cell mediated glomerular inflammation followed by 2) severe fibrocellular/fibrous crescent formation. Female Wistar-Kyoto rats (4-6wks old) were used (n=10 treatment group, n=10 control group). Anti-GBM disease was induced with peptide in treatment group, while controls were immunized with vehicle solution only. At post-immunization days 26, 28, 33 and 38, anti-OPN was administered to treatment group. Animals were sacrificed at day 40. Kidneys were submitted for histopathologic (H&E, PAS, trichrome) and ultrastructural study.

Results: Anti-OPN markedly reduced fibrocellular/fibrous crescent formation. Animals with anti-OPN treatment resulted in crescent formation in 39.7% of glomeruli compared with 86.6% for the untreated controls (P<.05). Fibrotic crescents in anti-GBM group had only limited to small areas adjacent to Bowman's capsule affected versus global fibrotic crescent formation in controls. Global fibrotic crescents were not observed in anti-GBM group. Interstitial tissues were more severely affected in controls compared with anti-GBM group. Electron microscopy showed marked thickening, wrinkling of GBMs, foot process effacement, and mesangial matrix expansion with control group; while anti-GBM group had minimally thickened. wrinkled GBMs, less prominent mesangial matrix expansion, but foot process effacement. No electron dense deposits were noted with control or anti-GBM groups.

Conclusions: Anti-OPN treatment resulted in a marked reduction in fibrocellular/fibrotic crescent formation in an anti-GBM animal model with established crescentic disease, indicating that OPN may be a therapeutic target in anti-GBM disease and other crescentic glomerular diseases.

1954 Surfactant Deficiency Disorders: Review of Histopathologic and Ultrastructural Features.

J Hicks, C Langston, E Wartchow, G Mierau. Texas Children's Hospital & Baylor College of Medicine, Houston; The Children's Hospital, Denver, CO.

Background: Surfactant is comprised of phospholipids and proteins packaged in lamellar bodies and secreted by alveolar type II pneumocytes. There are 4 surfactant-associated proteins (SP-A, SP-B, SP-C, SP-D) and a phospholipid transporter (ABCA3). SP-B, SP-C and ABCA3 gene mutations are associated with respiratory disease in children.

Design: 2 pediatric hospital archives identified 29 patients with surfactant deficiencies (2 SP-B, 11 SP-C, 16 ABCA3). Clinical features for SP-B deficiency were respiratory distress (RDS) shortly after birth requiring mechanical ventilation, and chest radiograph with diffuse haziness and air bronchograms. Clinical features of SP-C deficiency were variable. Some presented in the newborn period with RDS, indistinguishable from SP-B. Others presented in infancy and early childhood with gradual onset of respiratory insufficiency, hypoxemia, failure to thrive and interstitial lung disease. ABCA3 deficiency typically presented in the newborn period with RDS. Lung biopsies were performed and evaluated by routine histologic and electron microscopic (EM) techniques.

Results: SP-B deficiency showed alveolar wall widening without inflammation, mild to moderate alveolar epithelial hyperplasia, mild PAS positive intra-alveolar material, increased airspace macrophages, mild to minimal alveolar proteinosis, and no remodeling. EM showed lack of tubular myelin, disorganized lamellar bodies and irregular multivesicular bodies. SP-C deficiency shared features with chronic pneumonitis of infancy, lipoid pneumonia and cholesterol pneumonia, with alveolar wall widening with prominent alveolar epithelial hyperplasia, increased structural cells, mild chronic inflammation, and PAS positive globules, macrophages, eosinophils and cholesterol clefts in alveolar spaces. EM showed normal lamellar bodies and infrequent disorganized lamellar bodies. ABCA3 deficiency showed features overlapping with desquamative interstitial pneumonitis, pulmonary alveolar proteinosis, and nonspecific interstitial pneumonitis, with lobular remodeling, increased alveolar macrophages, pneumocyte hyperplasia, alveolar proteinosis (neonates and infants) and cholesterol clefts. EM showed small lamellar-like bodies with concentric phospholipid membranes and eccentric dense cores.

Conclusions: Ultrastructural findings associated with lamellar body formation in SP-B and ABCA3 are distinctive and distinguish these conditions from SP-C. These findings may guide genetic testing for the specific mutation responsible for the child's underlying respiratory disease.

1955 The Characteristics of Ultrastructural Findings of Muscle Biopsy from Early Onset Leigh Syndrome; the Proposal of Ultrastructural Diagnostic Criteria for Muscle Biopsy.

D Kim, SH Kim, S Noh, Y-M Lee. Yonsei University Health System, Seoul, Republic of Korea.

Background: Leigh syndrome, a devastating neurodegenerative disorder, can be broadly classified into two categories according to its onset -- early and late. There are no reliable morphological (ultrastructural) diagnostic criteria especially for early onset Leigh syndrome, probably reflecting a lack of sufficient chronological time to accumulate various morphologic alterations from mitochondrial dysfunction.

Design: To identify ultrastructural findings, which make it easier to diagnose early onset Leigh syndrome, from muscle biopsies, sixty-two cases clinically suspicious for Leigh syndrome are collected ranging in age from 0 to 10. Among many suggestions by Kyriacou, several categorical features (inflammatory cell infiltration, ragged red fiber, reticular pattern, increased glycogen, increase lipid, maximal longitudinal and transverse size, and presence of abnormal mitochondria, etc.) are selected to minimize inter- and intra-observer variations. Chi-square test and logistic regression are performed.

Results: The EM features including 'more than 3 layers of mitochondria in the subsarcolemmal area' and 'more than 2 layers of mitochondria in the intermyofibrillar area' were shown to be statistically significant in early onset Leigh syndrome group with specificity of 67% and sensitivity of 72%.

Conclusions: Several charateristical ultrastructural findings provided by this pilot study will be helpful to diagnose early onset Leigh syndrome.

1956 Hepatitis C Viral Load and Its Correlation with Histologic Grade of Inflammation and Ultrastructural Features.

SD Norwood, G Sidhu, N Cassai, G-Y Yang. Northwestern University Feinberg School of Medicine, Chicago, IL; New York University School of Medicine & New York VA Hospital, NY.

Background: The host immune response induced by the hepatitis C virus (HCV) plays a predominant role in the pathogenesis of HCV, leading to inflammation, fibrosis, and sometimes eventual cirrhosis. Whether or not HCV directly causes cytopathic injury is not clear. In our previous study, we showed that HCV induces unique ultrastructural organelles called autophagosomes. In the present study, we further examine the relationship of HCV viral load to both the histologic grade of inflammation and stage of fibrosis as well as the electron microscopic (EM) findings in liver biopsies of HCV patients.

Design: 30 cases of HCV hepatitis liver biopsies were collected and the histologic grading of HCV hepatitis was determined using the following parameters on a scale of 0-4: portal inflammation (PI), piecemeal necrosis (PN) and stage of fibrosis. EM was also performed and the amount of HCV-induced autophagosomes graded on a scale of 0-3. HCV viral load (VL) was obtained and patients were categorized as having either a high VL (HVL) with >500,000 copies/mL or low VL (LVL) with <500,000 copies/mL. The histologic and EM findings were then compared between the 2 groups.

Results: 9/30 (30%) cases had a LVL (2000-370,000 copies/mL) and 21/30 (70%) cases had a HVL (540,000->5,000,000 copies). Of the LVL cases, 44% (4/9) had a PN grade of ≥2, 33% (3/9) had a PI grade of ≥2, 22% (2/9) had a stage of fibrosis ≥2, and 67% (6/9) had ≥2+ autophagosomes. Of the HVL cases, 67% (14/21) had a PN grade of ≥2, 76% (16/21) had a PI grade of ≥ 2, 62% (13/21) had a stage of fibrosis ≥2, and 86% (18/21) had ≥2+ autophagosomes. Overall, the HVL cases showed an increase in PN, PI, fibrosis, and autophagosome formation. The differences between the LVL and HVL cases were statistically significant for PI (p<0.0419).

Conclusions: Our results indicate the severity of portal inflammation is significantly correlated with HCV viral load. Although autophagosomes are a unique ultrastructural cytopathic change, the number of autophagosomes formed does not appear to be associated with viral load. Our results suggest the host immune-mediated inflammatory process together with direct viral cytopathic change is the crucial pathogenic process of hepatitis C.

1957 Ultrastructural Features of Transplant Glomerulopathy: The Role of Electron Microscopy in Early Diagnosis.

MA Raza, R Tashjian, H Qu. St. John Hospital and Medical Center, Detroit, MI.

Background: Transplant glomerulopathy (TG) is a pathologic condition of renal allografts that is now recognized as a distinct entity from other forms of chronic allograft damage.TG has been associated with circulating antidonor human leukocyte antigen (HLA) antibodies and the deposition of the complement split product C4d in peritubular capillaries (PTCs), suggesting antibody-mediated mechanism. The light microscopic alterations that develop during the course of this condition is characterized by double contours of glomerular basement membrane (GBM). Early TG is best identified by electron microscopy (EM), which can detect separation of endothelium from GBM before the establishment of GBM duplication and mesangial interposition. The purpose of this study was to determine the effectiveness of EM in the diagnosis of early TG.

Design: To assess the value of EM in early TG, we conducted a retrospective study on 162 graft biopsies obtained at our institution from 2008–2009. Each case was review by EM and interpretation was based on subendothelial space widening {Figure 1), GBM duplication (Figure 2), and mesangial interposition.

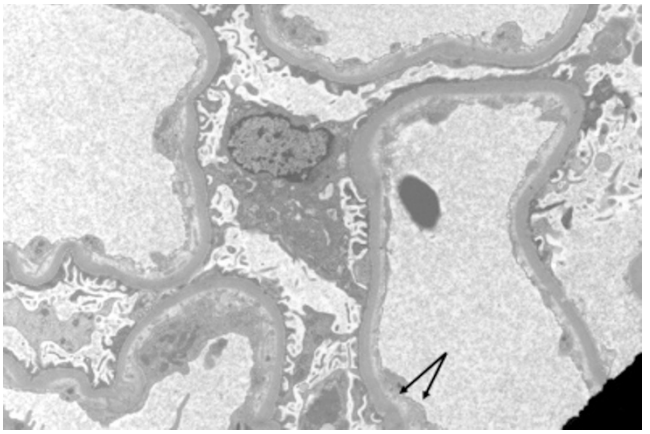

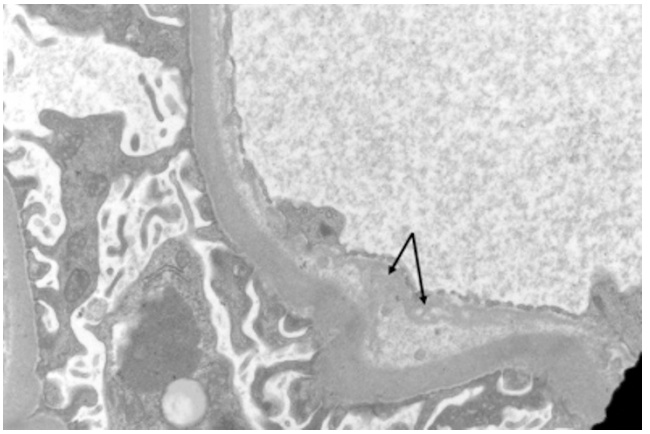

Results: Of the 162 biopsies, 58 (36%) exhibited TG by light microscopy, of which 47 (81%) demonstrated early developing TG as detected by EM. The remaining 115 biopsies were negative for TG by light microscopy, but EM unveiled evidence of TG in 13 (11%) of these cases. In addition, of the 47 cases of early TG, 34 (72%) stained positively with C4d in PTCs.
Conclusions: In summary, sole dependence upon light microscopy with periodic acid-schiff and silver special stains in the evaluation of TG may yield false positive or false negative results. Furthermore, positive staining of PTCs with C4d may not always be present in patients suffering from TG. Subendothelial space widening is the most reliable and reproducible feature of TG and is best detected by EM, even if examination by light microscopy is unremarkable.

1958 Light Chain Proximal Tubulopathy: Expanding the Pathologic Spectrum with Deposition of Crystalline-Like Inclusions in Glomeruli and Interstitium in Addition to Proximal Tubules.

SG Sharma, SM Bonsib, N Gokden. University of Arkansas for Medical Sciences, Little Rock; Louisiana State University Health Sciences Center, Shreveport.
Background: Light chain proximal tubulopathy (LCPT) is a rare form of renal disease associated with plasma cell dyscrasias. There are less than 100 cases reported in literature. The affected patients may present with proteinuria, kidney failure, Fanconi syndrome, or osteomalacia. The extent of dysproteinemia varies from monoclonal gammopathy of undetermined significance to overt multiple myeloma (MM). It is characterized by the deposition of crystallized monoclonal light chains in the cytoplasm of proximal tubules (PT). By immunofluorescence (IF) these crystals are predominately staining with kappa, and ultrastructurally, crystals are located within lysosomes. Rare cases of LCPT without crystalline-like inclusions only showed prominent phagolysosomes by EM. Our case series expand the existing literature with the involvement of glomeruli and interstitial cells by crystalline-like inclusions.
Design: Retrospectively, the renal biopsy data base at 2 institutions was searched for last ten years for LCPT. 5 cases with LCPT were found. Clinical, light microscopic (LM), IF and EM findings were reviewed in each case.
Results: The patient ages ranged from 38 to 81 years (mean: 57; median: 54); 4 were male and 1 was female. 1 patient presented with Fanconi syndrome, 2 with proteinuria and 1 with renal failure. 4 patients were diagnosed with MM (IGG, kappa type); 1 patient had AL amyloidosis. LM showed abundant PAS negative, pale pink cytoplasmic inclusions in PT cells in all cases. In 1 case cytoplasmic inclusions were present in the podocytes, endothelial and parietal cells as well. IF revealed strong kappa staining of cytoplasmic inclusions in 4 cases. EM showed electron dense rectangular, rhomboid, or needle- shaped crystals in PT cells in 3 cases (60%), 1 of which had crystals in mesangial, endothelial, visceral epithelial and interstitial cells as well. One showed prominent endolysosomes and one had amyloid fibrils only.
Conclusions: In a small number of LCPT cases crystalline-like inclusions may be deposited in glomerular and interstitial cells. It is important to be aware of these findings and look for the specific crystalline inclusions by LM, IF and EM in podocytes, endothelial, mesangial, parietal and interstitial cells in addition to PT epithelial cells. The mechanism of accumulation of these crystals in non-proximal tubular epithelial cell types and the significance of this finding are not clear.

1959 Ultrastructural Features of Unclassified Renal Cell Carcinoma: Implications for Tumor Re-Classification.

RV Talento, K Hewan-Lowe, M Yin. East Carolina University Brody School of Medicine, Greenville, NC.
Background: Unclassified renal cell carcinomas (URCCs) are malignant tumors that are morphologically unlike the recognized variations of the other established categories of renal cell carcinomas (RCCs). In concordance with the WHO 2004 classification, only those RCCs with apparent composites of recognized types, pure sarcomatoid morphology without recognizable epithelial elements, mucin production, rare mixtures of epithelial as well as stromal elements, and unrecognizable cell types that do not readily fit into one of the other known categories are assigned a diagnosis of URCC. URCC is an aggressive form of RCC because most cases are at an advanced stage at presentation, with higher rates of metastases and lower survival rates. Currently, there are no detailed reports on the ultrastructural features of URCCs or that address the impact of the ultrastructural features on the categorization of URCCs.
Design: The purpose of this study was to compare the ultrastructural findings of URCCs with those of the primary established categories of RCC (clear cell, papillary, chromophobe) and to determine whether there were ultrastructural features that would justify reclassification of a carcinoma assigned the diagnosis of URCC. Electron microscopy (EM) was performed on eight cases of high-grade renal tumors with solid growth patterns, without features of known RCC subtypes, urothelial carcinomas, or other recently described entities, such as mucinous tubular and spindle cell carcinoma or tubulocystic carcinoma of the kidney. The patients ranged in age from 49 years to 75 years (median 67 years). The range in maximum tumor dimension was from 3.3 cm to 20.0 cm (median 8.4 cm).
Results: Tumor cells of the examined URCCs show loss of cellular polarity with no apparent basal lamina. Rare, elongated desmosomal junctions and occasional tangled brush border-like microvilli are seen between the tumor cells. The cytoplasm shows abundant rough endoplasmic reticulum (RER) with no increased lipid or glycogen. Rare, rounded mitochondria and microvesicles are present. There are varying numbers of lysosomes of different sizes. Markedly irregular nuclei with prominent nucleoli are seen in the majority of cells.
Conclusions: The examined URCCs did not show ultrastructural morphology resembling the primary established categories of RCC or a specific line of tubular differentiation. The irregular nuclei and abundant RER were the major ultrastructural features observed, suggesting that URCCs are poorly differentiated renal carcinomas.

1960 The Reliability and Accuracy of Immuno-Gold Electron Microscopy for Subtyping Amyloid; Correlation with Laboratory Studies and Clinical Setting.

D Wang, J Lee, PT Soo Hoo, CJ O'Hara. Boston University Medical Center, Amyloid Treatment and Research Center, MA.
Background: Immuno-gold electron microscopy (EM) has shown promise as an additional modality for amyloid typing. The sensitivity and specificity of this modality has not been fully assessed due to the limited number of cases studied. This study analyzed 64 patients with systemic amyloidosis subtyped by immuno-gold-EM and assessed how often the subtype was corroborated by ancillary studies and clinical setting.
Design: Immuno-gold-EM was performed on 40 fat aspirates, 16 heart biopsies, 2 colon biopsies, 1 each of renal, gastric, duodenum, liver, tongue and lung using antibodies to amyloid A, AL-kappa, AL-lambda and TTR. The subtypes were then compared to the available data for routine IHC, isoelectric focusing for TTR mutations and clinical data including patients' history, immunoglobulin studies (serum protein electrophoresis, immunofixation, free light chain analysis), bone marrow plasma cell clonality and volume as well as the spectrum of organ involvement. Two-tailed p values<0.05 was considered significant in McNemar X^2 test for sensitivity and Fisher's exact test for the 2x2 table.
Results: 84.6% (54/64) of cases were successfully subtyped by immuno-gold-EM. There were 19 TTR, 23 AL-λ, 4 AL-κ, 4 AA and 4 mixed type with 2 cases of TTR coexisting with AL-κ, 1 case of TTR coexisting with AL-λ and 1 case of AA coexisting with AL-κ. The amyloid was subtyped in 32 of 40 cases (80.0%) of fat aspirates and 22 of 24 organ biopsies (91.7%) (p=0.297). In 23 cases in which initial amyloid typing was attempted by routine immunohistochemistry (IHC), 91.3% (21/23) were successfully subtyped by immuno-gold whereas only 8/23 cases (34.8%) could be subtyped by routine IHC alone (p=0.009). when compared to the laboratory data and clinical presentation, there was a very good corroboration with the specific amyloid subtype
Conclusions: 1. Immuno-gold-EM subtyping of amyloid is accurate and reliable.
2. Immuno-gold-EM can be successfully applied to fat aspirates as well as organ biopsies.
3. In the majority of cases evaluated, ancillary studies and the clinical setting supported the amyloid subtype determined by immuno-gold-EM.